Available online at www.sciencedirect.com

ScienceDirect

Ceramics International 40 (2014) 487–493

CERAMICS INTERNATIONAL

www.elsevier.com/locate/ceramint

Synthesis and characterization of $Pb(Mg_{1/3}Nb_{2/3})O_3$–$PbTiO_3$ relaxor ferroelectrics modified by $Ba(Mg_{1/3}Nb_{2/3})O_3$

Jinghan Gao[a], Qiang Li[a,*], Nengneng Luo[a], Qingfeng Yan[a], Yiling Zhang[b], Xiangcheng Chu[b]

[a]*Department of Chemistry, Tsinghua University, Beijing 100084, China*
[b]*State Key Laboratory of New Ceramics and Fine Processing, Tsinghua University, Beijing 100084, China*

Received 14 April 2013; received in revised form 5 June 2013; accepted 10 June 2013
Available online 24 June 2013

Abstract

$0.05Ba(Mg_{1/3}Nb_{2/3})O_3$–$(0.95-x)Pb(Mg_{1/3}Nb_{2/3})O_3$–$xPbTiO_3$ [0.05BMN–(0.95−*x*)PMN–*x*PT] relaxor ferroelectrics have been synthesized by solid-state reaction. Phase structure and microstructure were characterized by means of X-ray diffraction and scanning electron microscopy (SEM). Dielectricity, piezoelectricity and ferroelectricity were also investigated. A partial phase diagram for this system was established based on the X-ray diffraction and dielectric measurements. A morphotropic phase boundary (MPB) area was identified within the composition range of $x=0.33$–0.36. A maximum $d_{33}=585$ pC/N could be obtained in 0.05BMN–0.60PMN–0.35PT. With increasing PT content, the behavior of as-prepared ceramics gradually shifts from relaxor to normal ferroelectrics. This pseudo-ternary system also possesses an enhanced ferroelectricity compared to BMN–PT and BZN–PT.
© 2013 Elsevier Ltd and Techna Group S.r.l. All rights reserved.

Keywords: C. Dielectric properties; D. Perovskite; Morphotropic phase boundary

1. Introduction

Lead-based relaxor ferroelectrics with complex perovskite structure are widely used in multilayer capacitors, piezoelectric actuators and ultrasonic transducers due to their excellent dielectric and piezoelectric properties [1–3]. The chemical formula of formal lead-based perovskite structure are known as $Pb(B'\,B'')O_3$ (B′ stands for Mg^{2+}, Zn^{2+}, Ni^{2+}, Fe^{3+}, Sc^{3+}, In^{3+}, etc. B″ stands for Nb^{5+}, Ta^{5+}, W^{6+}, etc.) [4,5]. In order to stabilize the perovskite structure and enhance the electrical properties, a normal ferroelectric $PbTiO_3$ (PT) was introduced to relaxor ferroelectric $Pb(Mg_{1/3}Nb_{2/3})O_3$ (PMN) to form $Pb(Mg_{1/3}Nb_{2/3})O_3$–$PbTiO_3$ (PMN–PT) solid solution [6]. As a typical lead-based relaxor ferroelectric, PMN–PT with a morphotropic phase boundary (MPB) composition could possess $d_{33}=500$–600 pC/N, ~0.1% longitudinal strain, <0.05 $\tan\delta$ at room temperature, which constitute enabling performance for various military and commercial applications [7,8].

$Ba(Mg_{1/3}Nb_{2/3})O_3$ (BMN) is one of the best candidates for microwave dielectric material due to its low dielectric loss tangent and high dielectric constant [9,10]. Recently, Ba-$(Mg_{1/3}Nb_{2/3})O_3$–$PbTiO_3$ with a higher Curie temperature and modified dielectric property has been studied by Ye et al. [11]. Its dielectric constant at room temperature has increased dramatically (ε_r~4000) compared to non-doped BMN ceramic (ε_r~34) [11,12]. However, the effects of BMN doping on the MPB position and electrical properties of PMN–PT system still lack investigations.

Examination of the composition dependence of piezoelectric response in PMN–PT system indicates that higher dielectric and piezoelectric properties usually appear in the area close to MPB which separates the rhombohedral and tetragonal phases [13,14]. Strong interest has been developed in this area after "MPB" was first raised by Jaffe [4]. It is believed that PMN–PT with MPB composition is more electrically active because of more spontaneous polarization states which are more susceptible to an electric field drive, allowing optimum

*Corresponding author. Tel.: +86 10 62797871; fax: +86 10 62771149.
E-mail addresses: gjinghan@163.com.(J. Gao)
qiangli@mail.tsinghua.edu.cn.(Q. Li)

0272-8842/$ - see front matter © 2013 Elsevier Ltd and Techna Group S.r.l. All rights reserved.
http://dx.doi.org/10.1016/j.ceramint.2013.06.028

domain reorientation, and enhancing the piezoelectric performance [15,16]. In addition, an energy coupling effect between rhombohedral and tetragonal phases with MPB composition allowed such material to exhibit an ultrahigh coupling coefficient between its close energy states [17,18]. Therefore, it is crucial to learn more about the MPB region of PMN–PT modified by BMN.

Furthermore, according to Eitel's result, the phase transition temperature (T_c) of the MPB decreases linearly as the tolerance factor of the non-PT end members increases [19]. BMN should be controlled at a small amount as it has a very large tolerance factor ($t=1.03$) using Shannon's ionic radii [11]. In order to explore the MPB region in BMN–PMN–PT system, a small amount of BMN (5 mol%) doped PMN–PT (65/35) with MPB composition has been studied. Synthesis, structure analysis, piezoelectricity, dielectricity and ferroelectricity of the 0.05Ba$(Mg_{1/3}Nb_{2/3})O_3$–$(0.95-x)Pb(Mg_{1/3}Nb_{2/3})O_3$–$xPbTiO_3$ family have been discussed in the paper. The partial phase diagram for BMN–PMN–PT pseudo-ternary system has revealed the existence of MPB area with good piezoelectric and dielectric properties.

2. Experimental procedure

Ceramics of 0.05BMN–$(0.95-x)$ PMN–xPT with $x=0.29$, 0.31, 0.33, 0.34, 0.35, 0.36, 0.37 and 0.39 were prepared by solid-state reactions as reported [7,20]. Starting materials were high-purity powders of $BaCO_3$, PbO, TiO_2, MgO and Nb_2O_5 (99.99%). To avoid the pyrochlore phase which would degrade the dielectric and electromechanical properties, a two-step processing was adopted [21]. First, the stoichiometric ratio of MgO and Nb_2O_5 were ball-milled and calcined at 1100 °C for 4 h to obtain precursor $MgNb_2O_6$ (MN). Then MN, PbO, TiO_2 and $BaCO_3$ were mixed and ball-milled according to the stoichiometric ratio. The mixtures were calcined at 850 °C for 4 h to form perovskite powders. As-prepared 0.05BMN–$(0.95-x)$PMN–xPT powders were pressed as disc-shaped pellets under a pressure of 7 MPa with 5 wt% polyvinyl alcohol (PVA) as a binder. As-pressed pellets were sintered at 1150–1200 °C. After that, both the circular surfaces of ceramic samples were polished and coated with silver as electrodes. XRD (D8 ADVANCE Brüker, German) was applied to identify the crystal structure. Microstructure was observed by scanning electron microscopy (Quanta 200 FEG; FEI Company, Eindhoven, The Netherlands). The dielectric properties of silver-coated specimens were measured as a function of temperature by an Agilent 4294A impedance analyzer with Delta 9023 from 25 °C to 220 °C. The ceramics were poled under 3 kV/mm DC fields at various temperatures from 90 °C to 120 °C according to the T_c. A quasistatic piezo-d_{33} meter (Institute of Acoustics, Chinese Academy of Science, ZJ-4J) was introduced to explore its piezoelectric contents (d_{33}).

3. Results and discussion

Fig. 1(a) is the X-ray diffraction patterns of as-sintered 0.05BMN–$(0.95-x)$PMN–xPT ceramics with selected compositions of $x=0.29-0.39$. It indicates that all samples with

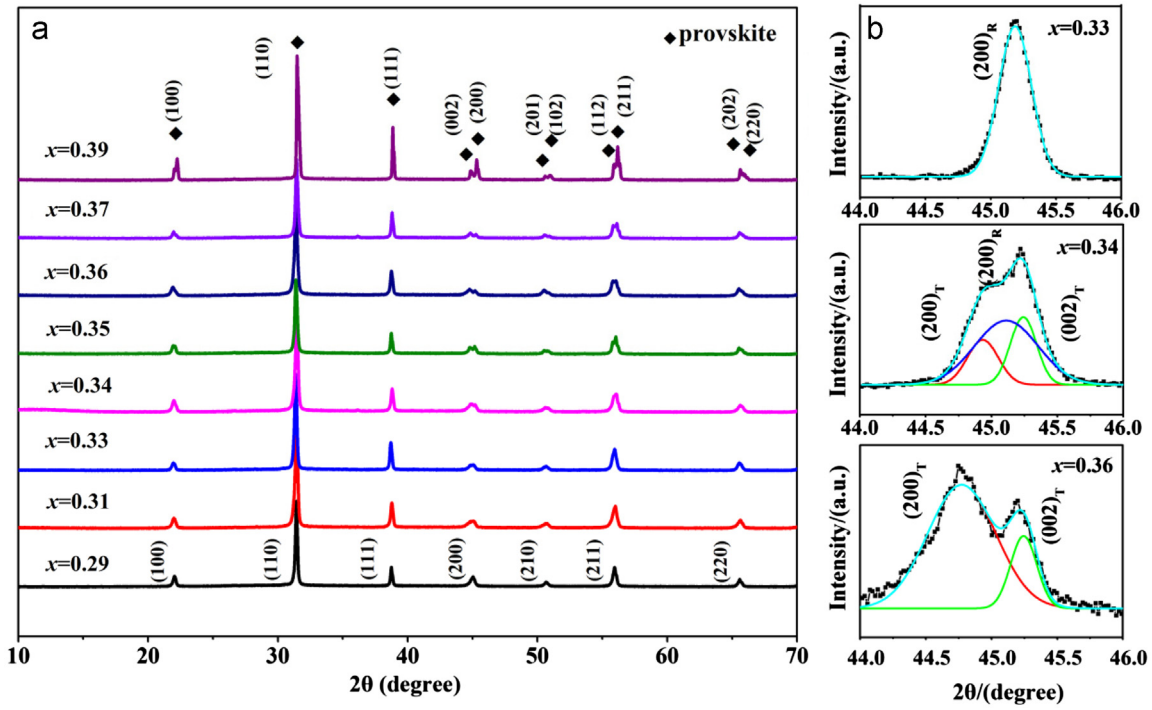

Fig. 1. (a) XRD patterns of as-sintered ceramics with various compositions 0.05BMN–$(0.95-x)$PMN–xPT ($x=0.29$, 0.31, 0.33, 0.34, 0.35, 0.36, 0.37 and 0.39). (b) Fitting results of peaks near $2\theta=45^{o}$ with compositions of 0.05BMN–$(0.95-x)$PMN–xPT ($x=0.33$, 0.34, and 0.36).

different compositions are of pure perovskite phase. In addition, the diffraction peaks shift to higher 2θ angle with increasing x values. The lattice parameters can be determined by Bragg's relation of $d=n\lambda/2\sin\theta$ [22]. It is acknowledged that the radius of Ti^{4+} (60.5 pm) is smaller than that of Mg^{2+} (72 pm) and Nb^{5+} (64 pm), therefore the unit cell parameters become smaller as the result of increasing PT content. The compositions with $x\leq0.33$ exhibit a rhombohedral phase with a single peak $(200)_R$. While samples with compositions of $x=0.36$ and higher show the splitting of (200) peak, suggesting that their structures change to be tetragonal phase with only $(200)_T$ and $(002)_T$ exist. For $x=0.33$–0.36, the (200) peak first becomes broaden and asymmetrical, and then splits at $x=0.36$, indicating that the symmetry of the phase gradually changes from rhombohedral to tetragonal with increasing PT content from $x=0.33$ to 0.36. Therefore, a morphotropic phase boundary (MPB) is probably located within a composition range of $0.33<x<0.36$.

Fig. 1 (b) shows the experimental XRD data and fitting results of peaks 2θ near 45°. It can be found that, for $x=0.33$, the (200) peak is composed of a single peak, corresponding to the rhombohedral phase. For $x=0.34$, the (200) peak is composed of three peaks, with dominant broaden peak $(200)_R$ corresponding to the rhombohedral phase and the other two weak peaks $(200)_T$ and $(002)_T$ corresponding to the tetragonal phase. For $x=0.36$, the tetragonal phase can be identified by two distinct peaks $(200)_T$ and $(002)_T$ while $(200)_R$ peak disappears. This result also indicates that there is a coexistence of rhombohedral and tetragonal phases within the MPB area ($0.33<x<0.36$).

The SEM of synthesized compositions sintered at 1150–1200 °C for 4 h are shown in Fig. 2. It indicates that the grain sizes of as-sintered ceramics vary from 2 to 10 μm. Ceramics of $x=0.35$, located within the MPB area, possesses the largest grain size. And the coexistence of transgranular fracture and intergranular fracture demonstrates that the sintering temperature is appropriate.

Fig. 3 is the dielectric properties of 0.05BMN–(0.95−x)PMN–xPT ceramics at the frequency of 1 kHz for the selected compositions of $x=0.29$, 0.31, 0.33, 0.34, 0.35, 0.36, 0.37 and 0.39. A broaden peak of dielectric constant appears at $x=0.29$, and then turns to be sharper with increasing PT content, indicating a gradual transformation from relaxor ferroelectrics to normal ferroelectrics. The inset of Fig. 3 shows the variations of T_c with different PT content. T_c of as-sintered ceramics is about 106 °C when x value is 0.29, while it increases almost linearly as a function of PT content. It can even reach up to 150 °C when x is 0.39. After fitting by the least squares method, an equation is attained about the relationship between T_c and PT content (x).

$$T_c = 4.6x - 25.8\ (^{\circ}C) \tag{1}$$

From this fitting result, it can be gained that the slope of curve is about 4.6 °C/mol%, which is a little bit different from the previously research [23]. This may be attributed to the introduction of BMN with a relatively lower T_c, comparing with PT. Doping a component with lower T_c will in turn decrease the phase transition temperature in perovskite structure [24].

The temperature dependence of dielectric constant (ε_r) for synthesized compositions is measured at various frequencies (1, 10, and 100 kHz) as shown in Fig. 4. It indicates that the dielectric constant first increases with increasing temperature and experiences a maximum at T_c, corresponding to ferroelectric and paraelectric phase transitions. When $x=0.33$, it exhibits a broaden dielectric peak, which indicates that as-sintered ceramics perform a relaxor behavior. With the increasing PT content, dielectric peaks become more and more sharper, which is related to a poor relaxor behavior. In order to determine the degree of relaxor behavior in a semi-quantitative way, the degree of diffuseness γ was put forward according to formula [12,25].

$$ln(1/\varepsilon_r - 1/\varepsilon_m) + \ln C = \gamma ln(T - T_m)\ (T > T_m) \tag{2}$$

Where ε_m is the maximum dielectric constant, C is a constant, T_m stands for the temperature at dielectric maximum, and γ is named as the degree of diffuseness of the phase transition with the value varying from 1 to 2. The insets of Fig. 4 are the fitting results obtained by the least squares method according to formula (2). It indicates that with the increasing PT content, γ has a decreasing tendency from 1.97 for $x=0.33$ to 1.64 for $x=0.39$, which can also be found in Table 1. In addition, $\Delta T_{diffuse}$ in Table 1 is also a parameter which is applied to testify the relaxor behavior. It is defined as the following equation [26]:

$$\Delta T_{diffuse(1kHz)} = T_{0.9\varepsilon_m(1\ kHz)} - T_{\varepsilon_m(1\ kHz)} \tag{3}$$

The calculated values of $\triangle T_{\mathrm{diffuse(1\ kHz)}}$ are listed in Table 1. The decreasing tendency of diffuseness implies that as-sintered ceramics change from typical relaxor to normal ferroelectrics.

Fig. 5 indicates the variation of piezoelectric coefficient (d_{33}) and planar mode electromechanical coupling coefficient (k_p) as a function of PT content. It can be found that d_{33} has a maximum value (585 pC/N) when $x=0.35$, which is even better than some of the PZT-based and PMN-based piezoelectric ceramics [27-29]. Both 0.33 and 0.36 have relatively higher d_{33} and k_p. This may be ascribed to the coexistence of rhombohedral and tetragonal phases near MPB area. It is believed that there are fourteen possible spontaneous polarization directions and close energy states at these two phases [30,31]. Furthermore, it has been confirmed that grain size is an important factor to affect piezoelectric property [32]. As mentioned in Fig. 2, samples with MPB compositions and larger grain sizes may also contribute to enhanced piezoelectric property.

The P–E loops of the 0.05BMN–(0.95−x)PMN–xPT ceramics measured at room temperature are shown in Fig. 6. All compositions exhibit well saturated P–E loops. It means that all as-sintered ceramics possess good ferroelectricity. The partial asymmetry of P–E loops may be attributed to the existence of internal strain and defect [21]. The values of remnant polarization (P_r) and coercive fields (E_c) obtained from Fig. 6 are shown in Table 2. It is found that the evaluated P_r first increases and then decreases when PT content increases.

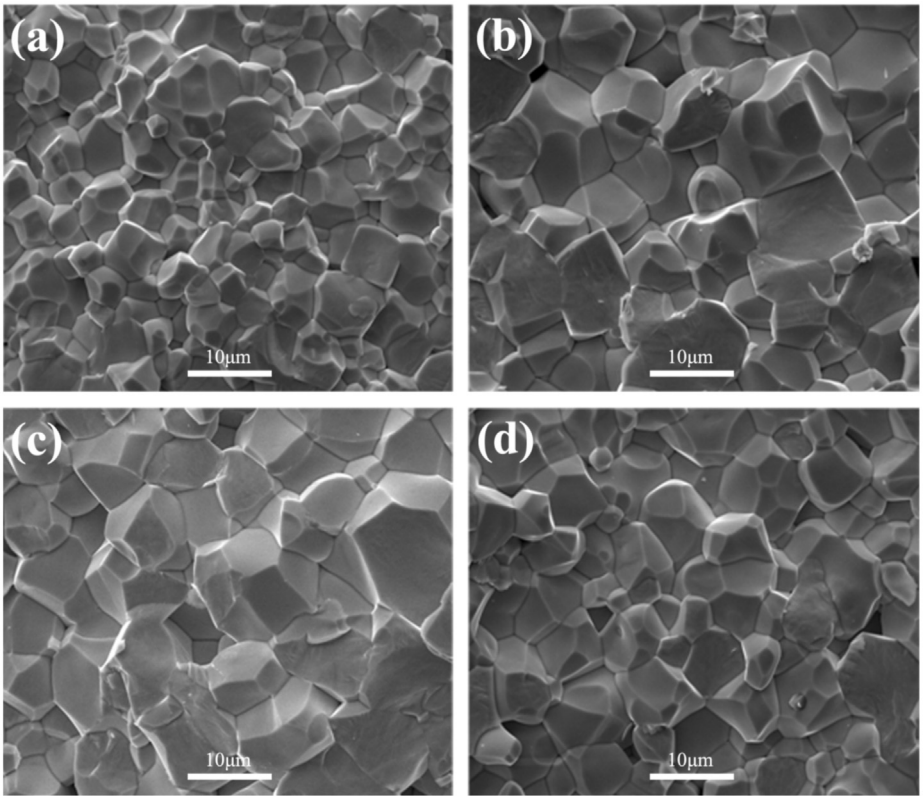

Fig. 2. SEM cross section photographs of 0.05BMN–(0.95−x)PMN–xPT ceramics sintered at 1150 °C–1200 °C for 4 h. (a) x=0.33, (b) x=0.35, (c) x=0.37, and (d) x=0.39.

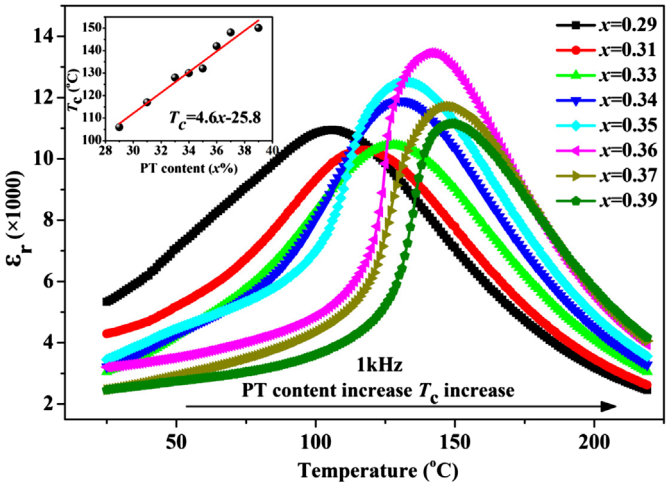

Fig. 3. Temperature dependence of dielectric constant of 0.05BMN–(0.95−x) PMN–xPT ceramics series at 1 kHz. The inset shows the tendency of T_c.

Both Table 2 and the inset of Fig. 6 have shown that the observed E_c increases linearly with increasing PT content. This may be related to the increase of tetragonal phase with PT content increasing, as the domain switching is more difficult in tetragonal than in rhombohedral phase [18]. Based on this analysis, it re-confirms that the tetragonal phase gradually increases with increasing PT content, which is well consistent with the previously phase analysis about X-ray results. Furthermore, comparing to BMN–PT and BZN–PT, BMN–PMN–PT possesses a much higher P_r of 20.3 μ/cm^2, indicating a better ferroelectric behavior [11,33]. And coercive field E_c is much lower than either BZN–PT (37/63) or BMN–PT (30/70), especially 6.4 kV/cm for x=0.35 [11,33]. This phenomenon is mainly ascribed to the lower PT content in BMN–PMN–PT within the MPB area than that of BMN–PT and BZN–PT. The larger proportion of rhombohedral phase in MPB composition allows BMN–PMN–PT to possess more spontaneous polarization states thus leading to optimum domain reorientation [11].

Fig. 7 is the partial phase diagram for 0.05BMN–(0.95−x) PMN–xPT pseudo-ternary system according to both the results of XRD and dielectric measurements. It demonstrates obviously that room-temperature phase structure transforms from the rhombohedral phase ($x < 0.33$) to coexistence of rhombohedral and tetragonal phases ($0.33 < x < 0.36$, MPB), then to tetragonal phase ($x > 0.36$). The diagram indicates a probably morphotropic phase boundary area (MPB), which is identified as the dividing line between two different adjacent phases.

For Pb(B′ B″)O_3–PT system, the PT content at MPB area exhibits a linear dependence on the radius and displacements of B cations. The MPB composition could be predicted by the following equation [34,35]:

$$x_{PT}^{MPB} = 1-1/(0.34 + 3.31R_B^{avg} - 7.49D_B^{avg}) \quad (4)$$

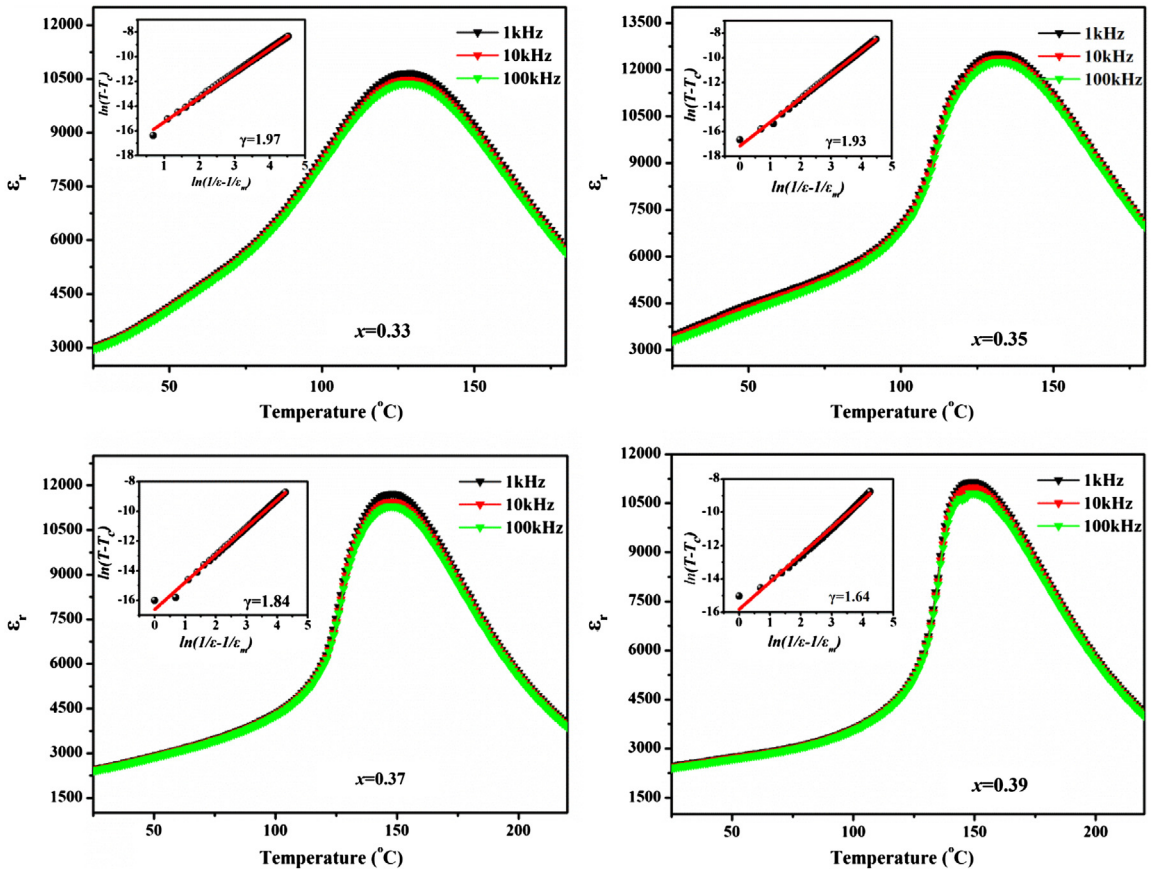

Fig. 4. Temperature dependence of dielectric constant (ε_r) of 0.05BMN–(0.95−x)PMN–xPT ceramics: (a) x=0.33, (b) x=0.35, (c) x=0.37, and (d) x=0.39. The inset shows the plots of $\ln(1/\varepsilon_r - 1/\varepsilon_m)$ vs. $\ln(T - T_c)$.

Table 1
Dielectric properties of BMN–PMN–PT ceramics.

Composition (x)	T_c (°C)	ε_m	ε_r at 25 °C	tanδ at 25 °C	Relaxor factor γ	$\Delta T_{diffuse}$ (°C)
0.29	106	10943	5335	0.026	1.97	20
0.31	117	10294	4292	0.015	1.95	19
0.33	128	10455	3061	0.029	1.97	19
0.34	130	11896	3216	0.009	1.96	14
0.35	132	12516	3452	0.014	1.93	14
0.36	142	11178	2583	0.007	1.91	13
0.37	148	11716	2469	0.006	1.84	13
0.39	150	11154	2461	0.008	1.64	11

Where x_{PT}^{MPB} is the mole fraction of PT at MPB, R_B^{avg} stands for the average ionic radius of the B cations in the non-PT end member, D_B^{avg} is the distortion magnitude for the B cations of the non-PT end member.

0.05BMN–(0.95−x)PMN–xPT and PMN–PT solid solutions have similar structures, both of which could be described as the chemical formula A(B′ B″)O_3–PT. The probable difference is that A means Ba^{2+} and Pb^{2+} in 0.05BMN–(0.95−x)PMN–xPT system. However, locating in A position, Ba^{2+} (135 pm) and Pb^{2+} (120 pm) have similar ionic radius and valence value. In this way, these two different solid solutions have similar A–B repulsion, which is considered to be a linear function of the ionic radius of the B cations. Therefore, the mole fraction

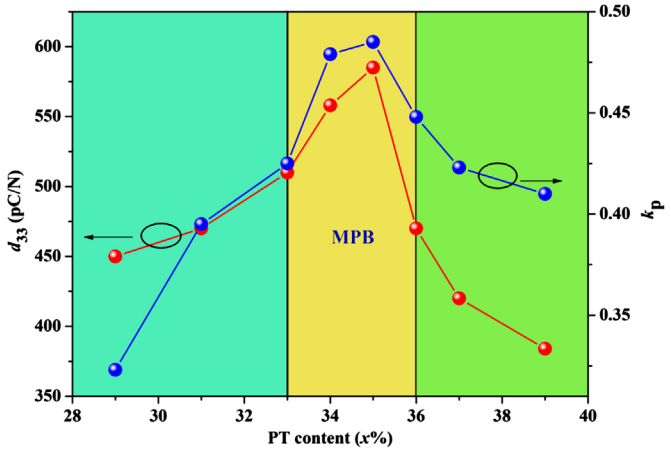

Fig. 5. Piezoelectric coefficient (d_{33}) and planar mode electromechanical coupling coefficient (k_p) of 0.05BMN–(0.95−x)PMN–xPT.

of PT at MPB for this novel pseudo-ternary system will follow the formula (4). In addition, the values of R_B^{avg} and D_B^{avg} can be obtained according to the data in the reference [34]. The calculated mole fraction of PT at MPB is $x_{PT}^{MPB} = 0.338$ for 0.05BMN–(0.95−x)PMN–xPT is generally in a good agreement with the experimental MPB compositions. In addition, the piezoelectric and ferroelectricity are in accordance with the MPB area ($0.33 < x < 0.36$).

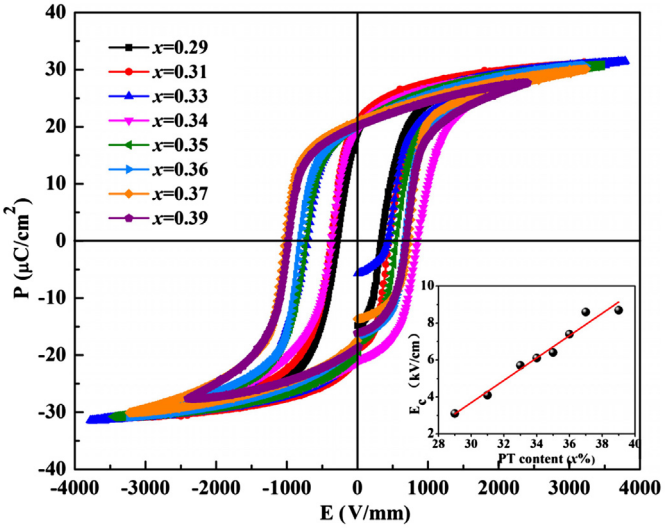

Fig. 6. The *P–E* hysteresis loops at room temperature of 0.05BMN–(0.95−*x*)PMN–*x*PT ceramics (*x*=0.29, 0.31, 0.33, 0.34, 0.35, 0.36, 0.37 and 0.39). The inset shows the tendency of E_c.

Table 2
Piezoelectricity and ferroelectricity of 0.05BMN–(0.95−*x*)PMN–*x*PT ceramics.

Composition (*x*)	d_{33} (pC/N)	k_p	P_r (μ/cm^2)	E_c (kV/cm)	
0.29	450	0.32	18.8	3.1	
0.31	470	0.40	18.9	4.1	
0.33	510	0.43	19.3	5.7	
0.34	558	0.48	20.3	6.1	This work
0.35	585	0.49	20.3	6.4	
0.36	470	0.45	19.7	7.4	
0.37	420	0.42	19.4	8.6	
0.39	384	0.41	19.3	8.7	
BMN–PT (30/70)	–	–	10	18	Ref. [11]
BZN–PT (37/63)	–	–	10	15	Ref. [34]

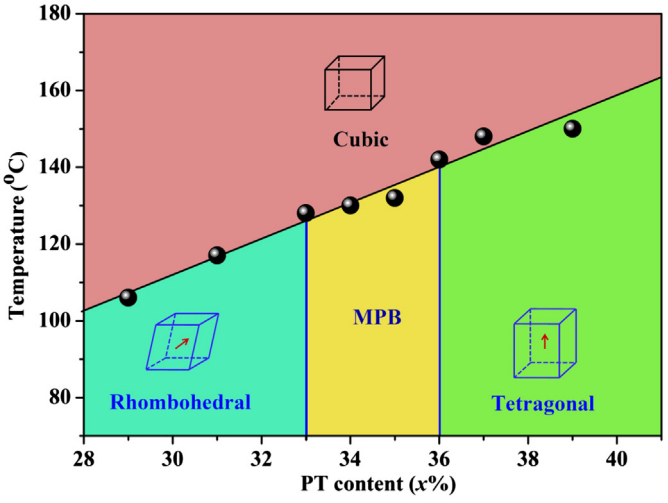

Fig. 7. Partial phase diagram for 0.05BMN–(0.95−*x*)PMN–*x*PT pseudo-ternary system.

4. Conclusions

0.05BMN–(0.95−*x*)PMN–*x*PT pseudo-ternary ceramics have been synthesized by solid state reaction and characterized by dielectric, piezoelectric and ferroelectric measurements. A partial solid state phase diagram of the ternary system has been established based on the structural and dielectric characterizations. A morphotropic phase boundary area is identified within a composition range of $0.33 < x < 0.36$. With the increasing PT content, as-sintered ceramics shift from typical relaxor ferroelectrics to normal ferroelectrics with a linear increase of T_c. As-sintered samples with MPB compositions exhibit d_{33}=585 pC/N, P_r=20.3 μ/cm^2, and E_c=6.4 kV/cm, which indicate comparable piezoelectric property with other lead-base piezoelectric ceramics and enhanced ferroelectricity than that of the BMN–PT and BZN–PT systems.

Acknowledgments

This work was supported by the National Basic Research Program of China (Grant No. 2013CB632900), the National Natural Science Foundation of China (Nos. 50972071 and 51172118) and the funds of State Key Laboratory of New Ceramics and Fine Processing, Tsinghua University, Beijing 100084, China.

References

[1] Z. Kutnjak, J. Petzelt, R. Blinc, The giant electromechanical response in ferroelectric relaxors as a critical phenomenon, Nature 441 (2006) 956–959.
[2] S. Zhang, W. Jiang, J.R.J. Meyer, F. Li, J. Luo, W. Cao, Measurements of face shear properties in relaxor-$PbTiO_3$ single crystals, Journal of Applied Physics 110 (2011) 064106–064111.
[3] Y. Zhang, G. Gao, H.L.W. Chan, J. Dai, Y. Wang, J. Hao, Piezo-phototronic effect-induced dual-mode light and ultrasound emissions from ZnS:Mn/PMN–PT thin-film structures, Advanced Materials, 24, 1729–1735.
[4] B. Jaffe, W.R. Cook, H. Jaffe, Piezoelectric Ceramics, Academics Press, New York, 1971.
[5] N.N. Luo, Y.Y. Li, Z.G. Xia, Q. Li, Progress in lead-based ferroelectric and antiferroelectric single crystals: composition modification, crystal growth and properties, CrystEngComm 14 (2012) 4547–4556.
[6] B.J. Fang, C.L. Ding, J. Wu, Q.B. Du, J.N. Ding, X.Y. Zhao, H.Q. Xu, H.S. Luo, Preparation of $Pb(Mg_{1/3}Nb_{2/3})O_3$–$PbTiO_3$ ceramics by reaction-sintering method and their electrical properties, The European Physical Journal Applied Physics 57 (2012) 30101–30108.
[7] T.Y. Koo, S.W. Cheong, Dielectric and piezoelectric enhancement due to 90°domain rotation in the tetragonal phase of $Pb(Mg_{1/3}Nb_{2/3})O_3$–$PbTiO_3$, Applied Physics Letters 80 (2002) 4205–4207.
[8] Y.S. Cho, C.H. Yoon, S.M. Pilgrim, Effects of chemical additives on high-field electromechanical properties of PMN–PT–BT ceramics, Ceramics International 31 (2005) 1025–1029.
[9] J.B. Lim, D.H. Kim, S. Nahm, J.H. Paik, H.J. Lee, Effect of B_2O_3 and CuO additives on the sintering temperature and microwave dielectric properties of $Ba(Mg_{1/3}Nb_{2/3})O_3$ ceramics, Materials Research Bulletin 41 (2006) 1199–1205.
[10] M.A. Akbas, P.K. Davies, Ordering-induced microstructures and microwave dielectric properties of the $Ba(Mg_{1/3}Nb_{2/3})O_3$–$BaZrO_3$ system, Journal of the American Ceramic Society 81 (1998) 670–676.

[11] X.F. Long, Z.G. Ye, New dielectric and ferroelectric solid solution of $(1-x)Ba(Mg_{1/3}Nb_{2/3})O_3$–$xPbTiO_3$ with morphotropic phase boundary, Chemistry of Materials 19 (2007) 1285–1289.

[12] X.F. Long, Z.G. Ye, Relaxor behavior in the solid solution between dielectric $Ba(Mg_{1/3}Nb_{2/3})O_3$ and ferroelectric $PbTiO_3$, Applied Physics Letters 90 (2007) 112905–112907.

[13] Z.G. Ye, Y. Bing, J. Gao, A.A. Bokov, P. Stephens, B. Noheda, G. Shirane, Development of ferroelectric order in relaxor $(1-x)Pb(Mg_{1/3}Nb_{2/3})O_3$–$xPbTiO_3$($0 \le x \le 0.15$), Physical Review B 67 (2003) 104104–104111.

[14] A.K. Singh, D. Pandey, Evidence for MB and MC phases in the morphotropic phase boundary region of $(1-x)[Pb(Mg_{1/3}Nb_{2/3})O_3]$–$xPbTiO_3$: a rietveld study, Physical Review B 67 (2003) 064102–064113.

[15] H. Fu, R.E. Cohen, Polarization rotation mechanism for ultrahigh electromechanical response in single-crystal piezoelectrics, Nature 403 (2000) 281–283.

[16] C. He, X. Li, Z. Wang, H. Tailor, Y. Liu, T. Li, X. Long, Ferroelectric ternary solid solution of $Pb(Mg_{1/3}Nb_{2/3})O_3$–$PbSnO_3$–$PbTiO_3$ with morphotropic phase boundary, Ceramics International 39 (2013) 853–856.

[17] Q. Wei, Z. Wang, X. Li, X. Long, Z.G. Ye, Morphotropic phase diagram and dielectric and ferroelectric properties of $(1-x)Ba(Sc_{1/2}Nb_{1/2})O_3$–$xPbTiO_3$ solid solution, Chemistry of Materials 21 (2009) 506–510.

[18] T.R. Shrout, S.J. Zhang, Lead-free piezoelectric ceramics: alternatives for PZT?, Journal of Electroceramics 19 (2007) 113–126

[19] R.E. Eitel, C.A. Randall, T.R. Shrout, P.W. Rehrig, W. Hackenberger, S.E. Park, New high temperature morphotropic phase boundary piezoelectrics based on $Bi(Me)O_3$–$PbTiO_3$ ceramics, Japanese Journal of Applied Physics 40 (2001) 5999–6002.

[20] Z. Xia, L. Wang, W. Yan, Q. Li, Y. Zhang, Comparative investigation of structure and dielectric properties of $Pb(Mg_{1/3}Nb_{2/3})O_3$–$PbTiO_3$ (65/35) and 10% PbZrO3-doped $Pb(Mg_{1/3}Nb_{2/3})O_3$–$PbTiO_3$ (65/35) ceramics prepared by a modified precursor method, Materials Research Bulletin 42 (2007) 1715–1722.

[21] N.N. Luo, Q. Li, Z.G. Xia, Effect of $Pb(Fe_{1/2}Nb_{1/2})O_3$ modification on dielectric and piezoelectric properties of $Pb(Mg_{1/3}Nb_{2/3})O_3$–$PbZr_{0.52}Ti_{0.48}O_3$ ceramics, Materials Research Bulletin 46 (2011) 1333–1339.

[22] X. Zhao, W. Qu, X. Tan, A.A. Bokov, Z.G. Ye, Influence of long-range cation order on relaxor properties of doped $Pb(Mg_{1/3}Nb_{2/3})O_3$ ceramics, Physical Review B 79 (2009) 144101–144112.

[23] P. Kumar, C. Prakash, O.P. Thakur, R. Chatterjee, T.C. Goel, Dielectric, ferroelectric and pyroelectric properties of PMNT ceramics, Physica B: Condensed Matter 371 (2006) 313–316.

[24] J.D. Bobić, M.M. Vijatović Petrović, J. Banys, B.D. Stojanović, Electrical properties of niobium doped barium bismuth-titanate ceramics, Materials Research Bulletin 47 (2012) 1874–1880.

[25] A. Aoujgal, W.A. Gharbi, A. Outzourhit, H. Ahamdane, A. Ammar, A. Tachafine, J.C. Carru, Relaxor behavior in $(Ba_{1-3x/2}Bi_x)(Zr_yTi_{1-y})O_3$ ceramics, Ceramics International 37 (2011) 2069–2074.

[26] Y.D. Hou, N.N. Wu, C. Wang, M.K. Zhu, X.M. Song, Effect of annealing temperature on dielectric relaxation and Raman scattering of $0.65Pb(Mg_{1/3}Nb_{2/3})O_3$–$0.35PbTiO_3$ system, Journal of the American Ceramic Society 93 (2010) 2748–2754.

[27] C. He, X.Z. Li, Z.J. Wang, Y. Liu, D.Q. Shen, T. Li, X.F. Long, Phase diagram and electrical properties of $Pb(Yb_{1/2}Nb_{1/2})O_3$–$Pb(Mg_{1/3}Nb_{2/3})O_3$–$PbTiO_3$ ternary ceramics, Materials Research Bulletin 48 (2013) 131–136.

[28] J.S. Lee, M.S. Choi, N.V. Hung, Y.S. Kim, I.W. Kim, E.C. Park, S.J. Jeong, J.S. Song, Effects of high energy ball-milling on the sintering behavior and piezoelectric properties of PZT-based ceramics, Ceramics International 33 (2007) 1283–1286.

[29] R. Zhang, Z.P. Yang, X.L. Chao, C. Kang, Effects of CeO_2 addition on the piezoelectric properties of PNW–PMN–PZT ceramics, Ceramics International 35 (2009) 199–204.

[30] N.N. Luo, Q. Li, Z.G. Xia, X.C. Chu, Phase diagram, temperature stability, and electrical properties of $(0.85-x)Pb(Mg_{1/3}Nb_{2/3})O_3$–$0.10Pb(Fe_{1/2}Nb_{1/2})O_3$–$0.05PbZrO_3$–$xPbTiO_3$ system, Journal of the American Ceramic Society 95 (2012) 3246–3253.

[31] B.J. Fang, R.B. Sun, Y.J. Shan, K. Tezuka, H. Imoto, Phase transition, structural and electrical properties of $Pb(Zn_{1/3}Nb_{2/3})O_3$-doped $Pb(Ni_{1/3}Nb_{2/3})O_3$–$PbTiO_3$ ceramics prepared by solid-state reaction method, Journal of Physics and Chemistry of Solids 70 (2009) 893–899.

[32] L.B. Kong, T.S. Zhang, J. Ma, F. Boey, Progress in synthesis of ferroelectric ceramic materials via high-energy mechanochemical technique, Progress in Materials Science 53 (2008) 207–322.

[33] X.F. Long, Z.G. Ye, Morphotropic phase diagram and dielectric and ferroelectric properties of $(1-x)Ba(Zn_{1/3}Nb_{2/3})O_3$–$xPbTiO_3$ solid solution, Journal of Applied Physics 101 (2007) 124101–124105.

[34] H.B. Yang, C.R. Zhou, X.Y. Liu, Q. Zhou, G.H. Chen, H. Wang, W.Z. Li, Structural, microstructural and electrical properties of $BiFeO_3$–$BaTiO_3$ ceramics with high thermal stability, Materials Research Bulletin 47 (2012) 4233–4239.

[35] I. Grinberg, M.R. Suchomel, P.K. Davies, A.M. Rappe, Predicting morphotropic phase boundary locations and transition temperatures in Pb- and Bi-based perovskite solid solutions from crystal chemical data and first-principles calculations, Journal of Applied Physics 98 (2005) 094111–094120.